

Inhomogeneous frozen states in the Swift-Hohenberg equation: hexagonal patterns vs. localized structures

Denis Boyer* and Octavio Mondragón-Palomino
*Instituto de Física, Universidad Nacional Autónoma de México,
 Apartado Postal 20-364, 01000 México D.F., México*

(Dated: November 24, 2018)

We revisit the Swift-Hohenberg model for two-dimensional hexagonal patterns in the bistability region where hexagons coexist with the uniform quiescent state. We both analyze the law of motion of planar interfaces (separating hexagons and uniform regions), and the stability of localized structures. Interfaces exhibit properties analogous to that of interfaces in crystals, such as faceting, grooving and activated growth or “melting”. In the nonlinear regime, some spatially disordered heterogeneous configurations do not evolve in time. Frozen states are essentially composed of extended polygonal domains of hexagons with pinned interfaces, that may coexist with isolated localized structures randomly distributed in the quiescent background. Localized structures become metastable at the pinning/depinning transition of interfaces. In some region of the parameter space, localized structures shrink meanwhile interfaces are still pinned. The region where localized structures have an infinite life-time is relatively limited.

PACS numbers: 89.75.Kd, 05.45.-a, 64.60.My, 68.35.Dv

I. INTRODUCTION

Spatial disorder is a generic feature of pattern formation. Whereas the simplest patterns that appear in numbers of physical or chemical systems driven out of thermodynamic equilibrium are periodic structures (such as stripes, squares or hexagons), in practice, many steady patterns observed in spatially extended systems are more complex and disordered at large scale [1, 2, 3]. Why disordered configurations spontaneously form (without the help of impurities or any quenched disorder) and do not asymptotically evolve with time toward more ordered states is still not fully understood.

For instance, systems where various (say, two) patterns of different symmetries coexist can easily lead to disordered states. A basic example is Rayleigh-Bénard convection of non-Boussinesq fluids, where hexagonal patterns bifurcate subcritically and are stable along with the uniform conductive state within a whole interval of Rayleigh numbers. In bistability regions, asymptotic configurations may be either homogeneous (containing a single phase) or heterogeneous, with both phases present and distributed in a non-regular way. Heterogeneous states have been identified experimentally in Rayleigh-Bénard convection [4, 5], vibrated granular materials [6], or Turing patterns and related gas-discharge systems [7]. Spatial disorder has been also proposed as a generic feature of pattern formation in ecosystems, as illustrated by vegetation patches in arid regions [8].

On the theoretical side, the usual nonlinear model equations for periodic patterns often predict metastable disordered states as well. Regarding bistable/subcritical patterns, a lot of attention has been devoted in the past

years to localized structures, that are axisymmetric isolated structures of well-defined shape and size immersed in a uniform quiescent background (of vanishing order parameter) [9, 10, 11, 12, 13, 14, 15]. Localized structures have been identified as a possible origin of disorder in bistable systems, as asymptotic steady states are in some case composed of many localized structures randomly distributed in space [8, 11, 12]. The stability of these “spatially chaotic” states, as opposed to periodic, can be explained by the particular nature of the effective pair interaction between two localized structures [9].

In the present paper, we consider the Swift-Hohenberg model for hexagonal patterns in the bistability zone mentioned above and study spatially more extended objects, namely, islands with hexagonal order surrounded by the quiescent background. A localized structure can be seen as a limiting case where such a domain is of very small size (of order λ_0 , the wavelength of the base pattern). An interesting question to ask is up to what point localized structures and large islands differ from each other, although they probably share closely related features. We therefore analyze in the following the dynamics of a planar interface separating an extended domain of hexagons and a uniform phase in the bistability region. Although interfaces have been relatively less studied than localized structures in this context [13], we show that they play a central role in the large time evolution of two-dimensional extended systems, and in the formation of heterogeneous disordered states.

After recalling a few known results on the weakly nonlinear regime (Section II), we show that in the nonlinear regime interfaces can either move (with two modes: expanding or shrinking domains), or be pinned, depending on the value of the main control parameter (Section III). The theoretical treatment is based on an extension of the usual amplitude equation formalism to include “non-adiabatic” effects, according to some ideas presented in

*Electronic address: boyer@fisica.unam.mx

[16, 17, 18, 19, 20, 21]. Some analogies of this system with interfaces in solid crystals are pointed out. The results are further confronted with numerical resolution of the Swift-Hohenberg equation in Section IV, where a dynamical diagram for interfaces is drawn in parameter space. In Section V, we discuss the stability of heterogeneous frozen states. We show that the stability region of localized structures only partially overlap the pinning regime of interfaces. We deduce that the existence of steady disordered configurations (and therefore of localized structures of infinite life-time) is possible in practice only in that pinning regime. Disordered frozen configurations obtained from random initial conditions can be of various types: they can contain localized structures, or localized structures and extended domains of hexagons (“mixed” disorder), or extended domains and no localized structures. Changing the control parameters can drive the system outside of the pinning zone, keeping localized structures stable: these are absorbed by growing domains and therefore become metastable. Conclusions are presented in Section VI.

II. MODEL AND KNOWN RESULTS ON INTERFACE MOTION

We consider a system described by a dimensionless local order parameter $\psi(\vec{r}, t)$, representing, for example, the mid-plane vertical velocity in convection problems. The spatio-temporal evolution of ψ in non-Boussinesq convection can be described by a generalized Swift-Hohenberg equation [22],

$$\frac{\partial \psi}{\partial t} = \epsilon \psi - \frac{\xi_0^2}{4k_0^2} (\Delta + k_0^2)^2 \psi + g_2 \psi^2 - \psi^3. \quad (1)$$

The parameter $\epsilon \ll 1$ is the main control parameter and represents the reduced Rayleigh number $(R - R_c)/R_c$, where R_c is the critical Rayleigh number. $k_0 \equiv 2\pi/\lambda_0$ is the characteristic wavenumber of the patterns, and ξ_0 the bare coherence length. In the case of convection, ξ_0 is of order k_0^{-1} , its precise value depending on the boundary conditions at the fluid layer. The coefficient g_2 of the quadratic term in Eq.(1) models the strength of non-Boussinesq effects; g_2 will be taken as positive in the following without restricting generality ($g_2 \ll 1$).

Equation (1), or close variants of it, have been studied in many contexts, for instance, to describe the microphase separation of asymmetric block-copolymer melts in the weak segregation limit [23] or for degenerate optical parametric oscillators [12]. Recently, a similar equation was introduced to describe the evolution of vegetation biomass (the local order parameter in that case) in arid climates [8].

Eq.(1) can be written under a frequently used form:

$$\frac{\partial \phi}{\partial T} = \Sigma \phi - (\Delta + k_0^2)^2 \phi + G_2 \phi^2 - \phi^3, \quad (2)$$

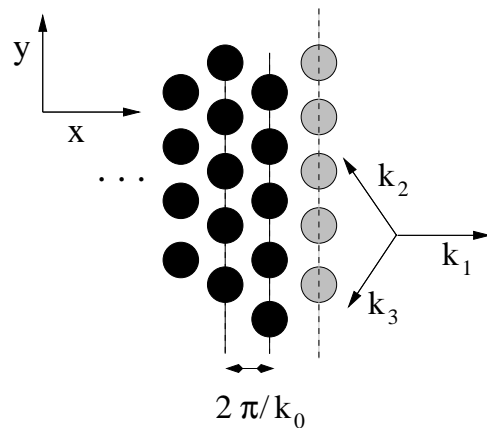


FIG. 1: Schematic representation of an interface between a hexagonal pattern (left) and a uniform state (right). The colors roughly represent the sign of ψ . The gray dots correspond to the next stable position of the interface in the pinning regime (see Section III B below).

with

$$\begin{aligned} \phi &= (\xi_0/2k_0)\psi, & T &= (\xi_0^2/4k_0^2)t, \\ \Sigma &= \epsilon/(\xi_0^2/4k_0^2), & G_2 &= g_2/(\xi_0/2k_0). \end{aligned} \quad (3)$$

We will take in the following ϵ and ξ_0 (rather than ϵ and g_2) as the two main tunable parameters of Eq.(1), g_2 being fixed to an arbitrary small value. The coherence length ξ_0 is thus considered as independent of λ_0 *a priori*. From (3), decreasing ξ_0 is equivalent to increasing the bifurcation parameters Σ and G_2 . Keeping $|\epsilon| \ll 1$, the weakly nonlinear regime corresponds to $\xi_0 \sim \lambda_0$, while the nonlinear regime is reached with $\xi_0 \ll \lambda_0$.

For $\epsilon < 0$, the uniform solution $\psi = 0$ (conductive state) is linearly stable, while it becomes unstable for $\epsilon > 0$. Standard weakly nonlinear analysis shows that a subcritical bifurcation to stable hexagonal patterns takes place at $\epsilon_m = -g_2^2/15 < 0$. Hexagonal patterns remain stable up to $\epsilon = 16g_2^2/3$, while stripes pattern become stable for $\epsilon \geq 4g_2^2/3$ [24]. In the following, we restrict our study to the coexistence zone of the hexagonal and conductive states ($\epsilon_m \leq \epsilon \leq 0$).

We come back in more details to a problem presented in [18]. We study a planar interface separating two semi-infinite domains, one composed of hexagonal patterns and the other in the uniform state $\psi = 0$. The local order parameter can be approximated at leading order ($\epsilon^{1/2}$) as

$$\psi_0 = \sum_{n=1}^3 A_n(x, t) \exp(i\vec{k}_n \cdot \vec{r}) + \text{c.c.}, \quad (4)$$

where the amplitudes A_n are slowly varying envelopes depending on x , the coordinate along the axis \hat{x} normal to the interface. The solutions of Eq.(1) satisfy the con-

dition

$$\lim_{x \rightarrow -\infty} A_n(x) = A_0 > 0, \quad \lim_{x \rightarrow \infty} A_n(x) = 0 \quad (n = 1, 2, 3). \quad (5)$$

The wave vectors \vec{k}_n are such that $|\vec{k}_n| = k_0$, and make an angle of $2\pi/3$ with each other. We choose \vec{k}_1 with an orientation perpendicular to the interface: this situation

corresponds a “faceted” hexagonal pattern having a row parallel to the interface, as schematically displayed in Fig.1. Faceted configurations are the more relevant ones, as further discussed in Section IV.

When $|\epsilon| \ll 1$, $g_2 \ll 1$ and $\xi \sim \lambda_0$, the equations satisfied by the amplitudes A_n can be derived from Eq.(1) by standard multiple scale analysis [3]:

$$\frac{\partial A_1}{\partial t} = \epsilon A_1 + \xi_0^2 \partial_x^2 A_1 + 2g_2 \bar{A}_2 \bar{A}_3 - 3(|A_1|^2 + 2|A_2|^2 + 2|A_3|^2) \quad (6)$$

$$\frac{\partial A_2}{\partial t} = \epsilon A_2 + \frac{\xi_0^2}{4} \partial_x^2 A_2 + 2g_2 \bar{A}_1 \bar{A}_3 - 3(|A_2|^2 + 2|A_1|^2 + 2|A_3|^2) \quad (7)$$

$$\frac{\partial A_3}{\partial t} = \epsilon A_3 + \frac{\xi_0^2}{4} \partial_x^2 A_3 + 2g_2 \bar{A}_1 \bar{A}_2 - 3(|A_3|^2 + 2|A_1|^2 + 2|A_2|^2), \quad (8)$$

(\bar{A} is the complex conjugate of A). Note that $A_3 = A_2$ from the planar geometry of the interface.

We next recall some known results on the velocity v of the interface. Use the ansatz $A_n = A_n(x - vt)$, multiply Eq.(6) (resp. Eqs.(7) and (8)) by $\partial_t \bar{A}_1$ (resp. $\partial_t \bar{A}_2$ and $\partial_t \bar{A}_3$), add the equations and integrate their real part over x . The velocity is obtained as [18]:

$$v = \frac{A_0^3 [45A_0/2 - 2g_2]}{2D}, \quad (9)$$

where A_0 is the amplitude of the regular hexagonal pattern

$$A_0 = \frac{g_2 + \sqrt{g_2^2 + 15\epsilon}}{15}, \quad (10)$$

and

$$D = \int_{-\infty}^{\infty} dx \sum_{n=1}^3 (\partial_x A_n)^2. \quad (11)$$

The numerator of Eq.(9) can be interpreted as a constant driving force acting on the interface, while D (which depends on the whole interface profile) plays the role of a friction term. The system of equations (6)-(8) has a potential form: there exists a functional “free-energy” $F \equiv \int d\vec{r} \mathcal{F}$ such that $\partial_t A_n = -\delta F / \delta \bar{A}_n$. The driving force in Eq.(9) (plotted below in Fig.2 as a function of ϵ) is proportional to the difference of free-energy density \mathcal{F} between the regular hexagonal state and the uniform state. Therefore, the sign of v is such that the domain with the lower free-energy expands at the expense of the other. From Eq.(9), g_2 being fixed, the velocity changes sign at $\epsilon = \epsilon_0 = -8g_2^2/135 = (8/9)\epsilon_m$, a value located in the coexistence region. The uniform phase spreads if $\epsilon_m \leq \epsilon < \epsilon_0$, whereas the hexagonal phase does in the much wider interval $\epsilon_0 < \epsilon \leq 0$. The interface is stationary only at $\epsilon = \epsilon_0$. Therefore, except at the marginal

value ϵ_0 , the amplitude equation formalism at leading order predicts that spatially heterogeneous distributions of hexagonal and conductive regions should eventually evolve toward a single state, either hexagonal or conductive, through interface motion.

III. NON-ADIABATIC EFFECTS

A. Modified amplitude equations

From Eqs.(6)-(8), the length scale of variation of the amplitudes, defining the interface thickness L , is roughly of order

$$L \sim \xi_0 / \sqrt{|\epsilon|} \quad \text{or} \quad \xi_0 / g_2. \quad (12)$$

Suppose now that $|\epsilon|$ (or g_2^2) is not that small compared to 1, and/or ξ_0 is significantly smaller than λ_0 : the assumption $L \gg \lambda_0$ may not be fulfilled in that case. The spatial variations of $A_n(x)$ are not necessarily much slower than the local oscillations of the patterns, and so-called “non-adiabatic” effects can appear. The effects of non-adiabaticity on moving interfaces have been studied theoretically for one-dimensional patterns [17, 20], stripe-stripe interfaces [21], square-hexagon interfaces [19], and other cases [18]. Non-adiabatic effects can be sufficient to pin interfaces and therefore to stabilize spatially heterogeneous configurations of the order parameter. A weakly nonlinear analysis taking into account these effects in the present case is reported in Appendix A. We derive the modified amplitude equations, with (small) non-adiabatic corrections that illustrate the coupling between the “fast” and “slow” length scales. Given the geometry depicted in Fig.1, one obtains

$$\frac{\partial A_1}{\partial t} = -\frac{\delta F}{\delta \bar{A}_1} - i\partial_x (g_2 A_1^2 - 6A_1 \bar{A}_2 \bar{A}_3) \frac{e^{ik_0 x}}{k_0} \quad (13)$$

$$+ i\partial_x [2g_2(|A_1|^2 + |A_2|^2 + |A_3|^2) - 6(A_1 A_2 A_3 + \bar{A}_1 \bar{A}_2 \bar{A}_3)] \frac{e^{-ik_0 x}}{k_0}$$

$$\frac{\partial A_2}{\partial t} = -\frac{\delta F}{\delta \bar{A}_2} + i\partial_x (2g_2 A_2 \bar{A}_1 - 3A_2^2 A_3 - 3\bar{A}_1^2 \bar{A}_3) \frac{e^{-ik_0 x}}{k_0} \quad (14)$$

$$A_3 = A_2. \quad (15)$$

In Eqs.(13)-(15), the $\delta F/\delta \bar{A}_i$'s are the right-hand sides of Eqs.(6)-(7).

The above equations involve directly the space variable x and therefore break the invariance by translation of standard amplitude equations. This is a consequence of the coupling between the amplitudes and the local phases of the waves. The additional terms in (13)-(15) can not be derived from a usual multiple scale analysis. Equations (13)-(15) have been derived in Appendix A in a lowest mode approximation (valid if L is still $\gg \lambda_0$): the non-adiabatic terms oscillate in that case with the same wavenumber than the base pattern, k_0 . Other terms oscillating as $\exp(2ik_0)$, $\exp(3ik_0)$... should be kept if $L \sim \lambda_0$, a situation corresponding to the strongly non-linear regime.

B. Pinned interfaces for ξ_0 of the order of $\xi_0^{(p)}$

Fixing the non-Boussinesq parameter g_2 to an arbitrary small value, we determine in this Section the finite

interval of values of the control parameter ϵ such that interfaces do not move, or are pinned. This interval depends on the coherence length ξ_0 , and can represent a significant part of the coexistence region when ξ_0 is small enough.

To derive the modified law of motion of the interface, we use the method described in Section II. Denoting x_0 the position of the interface and using the ansatz $A_n = A_n(x - x_0(t))$, one obtains from Eqs.(13)-(15),

$$v = \frac{dx_0}{dt} = \frac{F}{D} + \frac{p}{D} \sin(k_0 x_0) \quad (16)$$

$$\equiv -\frac{dV}{dx_0} \quad (17)$$

with

$$F = A_0^3[45A_0/4 - g_2], \quad (18)$$

and

$$p = \text{Max}_\varphi \int_{-\infty}^{\infty} dx \cos(k_0 x + \varphi) [A_1 \partial_x (3g_2 A_1^2 + 4g_2 A_2^2 - 18A_1 A_2^2) + 2A_2 \partial_x (2g_2 A_1 A_2 - 3A_2^3 - 3A_1^2 A_2)], \quad (19)$$

D being given by (11). In Eq.(16), the quantity p is a dimensionless positive number ($p \ll 1$) that can be identified with the magnitude of a periodic pinning potential: the motion of the interface is analogous to that of a viscous particle sliding down over an inclined plane with undulations. From Eq.(16), if $p \leq |F|$, the interface moves at speed $v \neq 0$, although non-constant in time. When $p \geq |F|$, the effective potential V seen by the interface has many local minima: there exist a set of discrete stable positions $x_0^{(p)}$ for which $v = 0$. The interface is pinned and hexagonal domains do not grow nor shrink. Two successive steady positions are separated by a distance λ_0 . This value for the periodicity (result of a single mode approximation, see Appendix A) has a simple geometri-

cal interpretation: the closest steady configuration of the faceted hexagonal domain represented in Figure 1 is the one obtained by addition (or symmetrically, removal) of an interfacial "layer" of dots parallel to the interface (the gray dots of Fig.1). This situation is analogous to that of a slow solidification (or melting) process controlled by activation barriers [26].

In expressions (11) and (19) we have assumed that the A_n 's are real (their imaginary part is supposed to be small). To evaluate p , we solve numerically the first order equations (6)-(7) for the moving interface, and substitute in (19). Although this solution is only approximate (in the pinning regime, we expect some changes in the amplitude profiles due to the fact that interfaces are

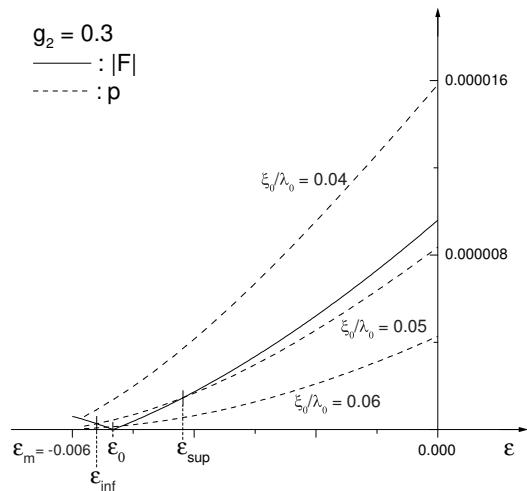


FIG. 2: Strength of the driving force F and of the pinning potential p (obtained for various values of the coherence length ξ_0) as a function of ϵ . $g_2 = 0.3$ here.

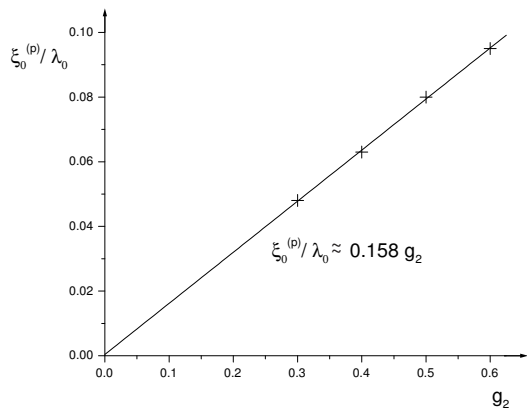


FIG. 3: Characteristic coherence length $\xi_0^{(p)}$, defining the onset of a significant pinning regime, as a function of g_2 , as given by weakly nonlinear analysis.

not moving), it captures the correct physical picture. A closer comparison with numerical solutions of Eq.(1) is performed in Section IV below.

In Figure 2, we plot the driving force $|F|$ and the pinning potential p given by Eqs.(18)-(19) as a function of ϵ , for a fixed value of g_2 . We show some curves of p obtained for different values of the coherence length ξ_0 (F is independent of ξ_0). Decreasing ξ_0 increases non-adiabatic effects and the pinning potential: from Eq.(19), p roughly behaves as

$$p \sim A_0^4 \exp(-aLk_0), \quad (20)$$

with a a numerical constant of order unity and L given by (12).

At fixed ξ_0 , interfaces are pinned in a range $\epsilon_{\text{inf}}(\xi_0) \leq \epsilon \leq \epsilon_{\text{sup}}(\xi_0)$, while hexagons shrink for $\epsilon_m \leq \epsilon \leq \epsilon_{\text{inf}}$ and expand for $\epsilon_{\text{sup}} \leq \epsilon$, see Fig.2. For $\xi_0 \sim \lambda_0$ (the

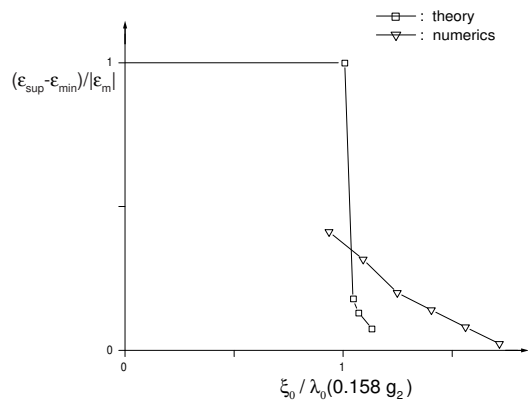


FIG. 4: Relative magnitude of the pinning interval as a function of $x = \xi_0/(0.158g_2\lambda_0)$, as given by weakly nonlinear theory and numerical solution of Eq.(1).

weakly nonlinear regime), the size of the pinning interval is extremely small compared with $|\epsilon_m|$, and limited to the vicinity of ϵ_0 . However, $\epsilon_{\text{sup}} - \epsilon_{\text{inf}}$ blows up and covers a significant part of the coexistence region at a cross-over value $\xi_0^{(p)} (< \lambda_0)$. The present calculation predicts that nearly the whole coexistence region (at least the interval $[\epsilon_0, 0]$) has pinned interfaces for ξ_0 smaller than a critical value (see Fig.2). We define the crossover value $\xi_0^{(p)}$ as given by this critical value. In Figure 3, we plot $\xi_0^{(p)}$ as a function of g_2 . A linear relation is observed:

$$\frac{\xi_0^{(p)}}{\lambda_0} \simeq 0.158 g_2. \quad (21)$$

Since $g_2 \ll 1$, $\xi_0^{(p)} \ll \lambda_0$ in Eq.(21). We conclude that pinning can be observed in practice only if the scale of variation of the amplitude is very short, corresponding to the *nonlinear* regime of Eq.(1), or equivalently if

$$G_2 \geq G_2^{(p)} \simeq 2k_0^2 \quad (22)$$

in Eq.(2). Unfortunately, in that regime, the equations (6)-(8) used to derive these results are no longer valid: higher order terms should be included to improve accuracy. We therefore do not expect this calculation to give a quantitative picture of pinning effects, but rather a qualitative one. An example of discrepancy between theoretical and numerical results (presented in the following Section) is that the predicted pinning in the nearly whole coexistence region at low ξ_0 is not observed numerically. Instead, pinning only occurs in the lower fraction of the coexistence interval, as further shown in Sec. IV below.

Nevertheless, the present weakly nonlinear analysis correctly captures the onset of a significant pinning regime for ξ_0 below a value $\xi_0^{(p)}$, as well as the right order of magnitude for $\xi_0^{(p)}$. In Figure 4, we plot the relative size of the pinning regime $(\epsilon_{\text{sup}} - \epsilon_{\text{inf}})/|\epsilon_m|$, determined from theory and numerics, as a function of

$x = \xi_0/(0.158g_2\lambda_0)$. Due to the exponential form of Eq.(20), the theoretical curve is nearly a step function at $x = 1$. The numerical curve is softer, but with significant variations around $x = 1$ as well.

IV. NUMERICAL RESULTS

A. Pinning of a planar interface

We numerically solve Eq.(1) by using a pseudo-spectral method and a time integration procedure described in [25]. The space is discretized on a square lattice, with 2048 nodes along \hat{x} , 128 nodes along \hat{y} , and periodic boundary conditions. The initial condition is a rectangular hexagonal domain of length 1028 and width 128, comprised in-between two quiescent regions of $\psi = 0$. The two interfaces are faceted and parallel to the \hat{y} direction. The lattice size Δx set to unity. The base period $\lambda_0 = 2\pi/k_0$ of the pattern is $4\sqrt{3}\Delta x$.

To determine whether interfaces are pinned or not, we compute the time evolution of the quantity

$$a(t) = \int_0^{l_x} \frac{dx}{\lambda_0} \int_0^{l_y} \frac{dy}{l_y} \psi^2, \quad (23)$$

with l_x and l_y the box dimensions. $a(t)$ is proportional to the length of the hexagonal domain, and therefore can be used to record the relative positions of the interfaces. Figure 5 shows transitions between moving and pinned boundaries as ϵ is decreased, for a given g_2 and ξ_0 . As expected, hexagonal domains are either expanding, steady or shrinking. In the moving regimes near a pinning transition, the motion is noticeably non-uniform in time, in agreement with the form of the law of motion (16).

Figure 6 displays a (ϵ, ξ_0) -diagram representing the pinned and moving regimes of hexagon/uniform interfaces. The parameter g_2 is fixed to 0.2, but the shape of the diagram is independent of this value, which just sets the scales of both axis (g_2^2 for the x -axis and g_2 for the y -axis, from Sections II and III). For comparison, we also report the characteristic values of ϵ given by weakly nonlinear analysis ($\xi_0 \sim \lambda_0$), introduced in Section II, and re-named $\epsilon_m^{(th)}$ and $\epsilon_0^{(th)}$ here. When $\xi_0 \ll \lambda_0$, the coexistence region delimited by the lower value ϵ_m becomes wider as ξ_0 decreases: ϵ_m deviates significantly from the value predicted by weakly nonlinear analysis. Yet, the picture drawn in the previous Section is qualitatively reproduced. At any ξ_0 , one can always identify two pinning-depinning transitions: For $\epsilon_m \leq \epsilon \leq \epsilon_{inf}$, hexagonal domains shrink; for $\epsilon_{inf} \leq \epsilon \leq \epsilon_{sup}$, interfaces are pinned; for $\epsilon_{sup} \leq \epsilon \leq 0$, hexagons expand. For ξ_0 small enough, the pinning interval ($\epsilon_{sup} - \epsilon_{inf}$) quickly grows from almost zero and becomes comparable to $|\epsilon_m|$. The numerical cross-over value found numerically compares well with that given by formula (21), as shown in Figure 4. The curve $\epsilon_m(\xi_0)$ converges toward the value $\epsilon_m^{(th)}$ as ξ_0 increases, while $\epsilon_{inf}(\xi_0)$ and $\epsilon_{sup}(\xi_0)$ converge toward

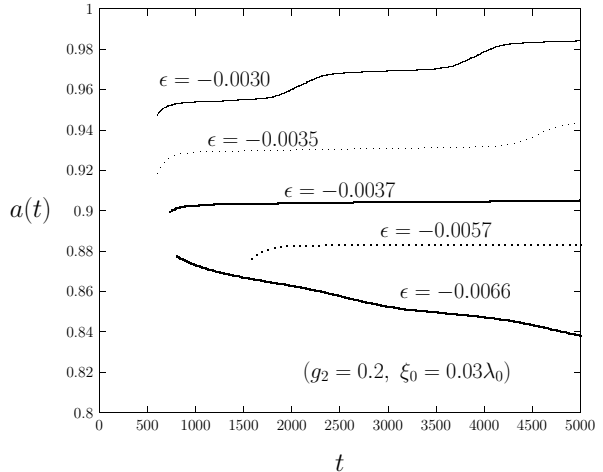


FIG. 5: Position of an interface as a function of time, obtained by numerical solution of Eq.(1), for various values of the control parameter ϵ . The two upper curves display a net motion over pinning barriers, the hexagonal domain expanding into the uniform region ($\epsilon > \epsilon_{sup} \simeq -0.0037$). The two following curves correspond to pinned interfaces ($\epsilon_{inf} < \epsilon < \epsilon_{sup}$), and the lower one to shrinking hexagonal domains ($\epsilon_m < \epsilon < \epsilon_{inf}$).

$\epsilon_0^{(th)}$. On the other hand, ϵ_m and ϵ_{inf} tend to merge as $\xi_0/\lambda_0 \rightarrow 0$, a trend also reproduced by the theoretical curves of Fig.2.

In the region located below the dotted line of Figure 6 (low ξ_0 and $|\epsilon|$), fronts are moving, with possible instabilities toward labyrinthine patterns or non-trivial uniform phases. This region is not of interest here and was not investigated.

B. Faceting of oblique interfaces

One can show from Section III that interfaces have to be faceted to be pinned. As detailed in the Appendix, if none of the wavenumbers \vec{k}_i of the base pattern is directed along the normal to the interface, the nonadiabatic terms (A2) will always integrate to zero along the transverse coordinate y . In [18], it was similarly argued that oblique interfaces could not be pinned. We show here that oblique interfaces actually modify their shapes to become pinned. More generally, in the pinning regime, an hexagonal domain surrounded by a conductive state $\psi = 0$ evolves toward a polygonal shape compatible with its three wavenumber directions. This situation can be seen as a nonequilibrium analogue of faceting in crystals due to strong anisotropy in surface tension [27].

As an example, we have solved numerically Eq.(1) with an initial condition composed of a planar interface with a wavenumber \vec{k}_1 making an angle $\theta = 5.73^\circ$ with the interface normal (Figure 7a). The interface evolves toward

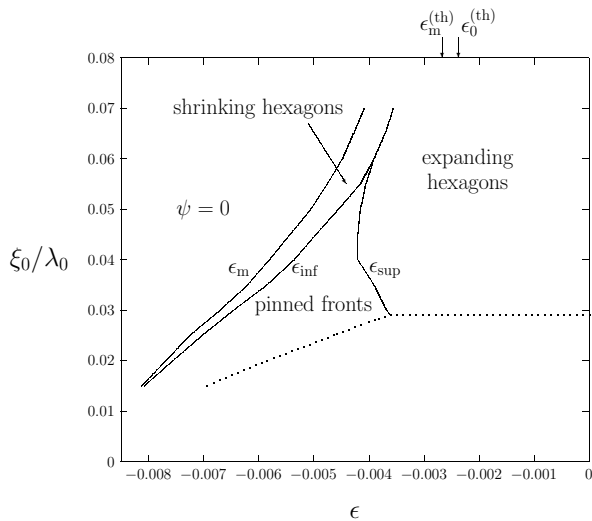


FIG. 6: Dynamics of hexagons/uniform interfaces in parameter space (ϵ, ξ_0) , for $g_2 = 0.2$. (The shape of the diagram does not depend on the value of g_2 , that only sets the scales of the axis.) The limiting values ϵ_m^{th} and ϵ_0^{th} given by weakly nonlinear analysis ($\xi_0/\lambda_0 \sim 1$) are reported for comparison. The region below the dotted curve is not of interest here, see text for details.

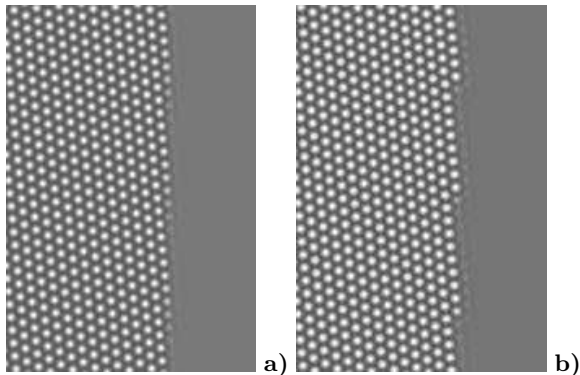


FIG. 7: Faceting of an oblique interface in the pinning regime ($g_2 = 0.2$, $\epsilon = -0.0041$, $\xi_0 = 0.03\lambda_0$). The initial interface makes an angle $\theta = 5.73^\circ$ with the normal. a) $t = 100$; b) $t = 1900$.

a wavy, faceted shape (Figure 7b).

V. DISORDERED STATES: COMPETITION BETWEEN DOMAINS OF HEXAGONAL ORDER AND LOCALIZED STRUCTURES.

From the preceding analysis, we conclude that spatially disordered configurations of the order parameter can be stabilized via pinning effects as soon as the coherence length is of order $\xi_0^{(p)}$ (or G_2 in Eq.(2) of order $G_2^{(p)}$, given by (22)). These configurations can contain immobile, extended hexagonal domains with faceted boundaries. In this subsection, we wish to compare the previously deter-

mined dynamical regimes for planar interfaces with the stability diagram of localized structures.

Localized structures are axisymmetric (dot-like) structures of well defined shape and size frequently encountered in bistability regions. They have been widely studied and have been recognized to play an important role in the production of disordered states [1, 9, 11]. The stability of assemblies of localized structures irregularly distributed in space is relatively well understood. The effective interaction force between two localized structures changes sign and oscillates with their separation distance (a property reminiscent of Eq.(16) for interfaces), therefore allowing many stable discrete positions that are unlikely to lead to periodic arrangements of structures [9]. We show below that the likelihood of observing localized structures in disordered solutions of Eq.(1) in fact largely depends on whether planar boundaries are pinned or not. We find that localized structures can actually coexist with pinned extended domains. In other cases, they are metastable, *i.e.* susceptible to be swept by any expanding domain of hexagonal order.

We have determined the stability diagram for a single localized structure. Calculations were performed on a square of 128×128 grid points over an extended period of time (20000 time units), and with a small additive noise term in Eq.(1). The initial localized structure (a region of size $\sim \lambda_0/2$ with $\psi > 0$) can either shrink, converge to a stable form, or expand. When localized structures expand, they generate hexagonal order, as described in details in refs. [7, 13]. Similarly to extended domains, we find that localized structures shrink if $\epsilon \leq \epsilon_{\text{inf}}^{(LS)}$, are stable if $\epsilon_{\text{inf}}^{(LS)} \leq \epsilon \leq \epsilon_{\text{sup}}^{(LS)}$, and expand if $\epsilon_{\text{sup}}^{(LS)} \leq \epsilon$. The results are reported in the (ξ_0, ϵ) -plane in Figure 8, together with the data of Figure 6 for planar fronts. Note that the stability zone of localized structures is located toward the right of the pinning regime of interfaces.

The stability interval $\epsilon_{\text{sup}}^{(LS)} - \epsilon_{\text{inf}}^{(LS)}$ and the pinning interval $\epsilon_{\text{sup}} - \epsilon_{\text{inf}}$ for boundaries become significant in the same range of values of the coherence length ξ_0 . The hatched region of Fig.8 indicates where both intervals overlap. In this region of parameters, localized structures actually have an infinite life-time. Anywhere outside this zone, localized structures are either unstable, or metastable, *i.e.* susceptible to be swept by a moving front of expanding hexagons. Also notice that when ξ_0/λ_0 is of order 1, $\epsilon_{\text{sup}}^{(LS)} (\simeq \epsilon_{\text{inf}}^{(LS)})$ tends to 0^- . Therefore, localized structures always shrink in the weakly nonlinear regime.

To further illustrate these results, we have solved the Swift-Hohenberg equation (1) with $g_2 = 0.2$ and random initial conditions, in various regions of Figure 8. For convenience, we fix $\xi_0 (= 0.031\lambda_0)$ in the vicinity of $\xi_0^{(p)}$. The initial condition for ψ is given by a random Gaussian field of zero mean and variance $\alpha^2 A_0^2$, with α a dimensionless tunable parameter of order 10.

Inside the hatched region of Figure 8 ($\epsilon_{\text{inf}}^{(LS)} \leq \epsilon \leq \epsilon_{\text{sup}}$) and with ϵ relatively closer to $\epsilon_{\text{inf}}^{(LS)}$, the asymptotic patterns obtained are mainly composed of aperiodic assem-

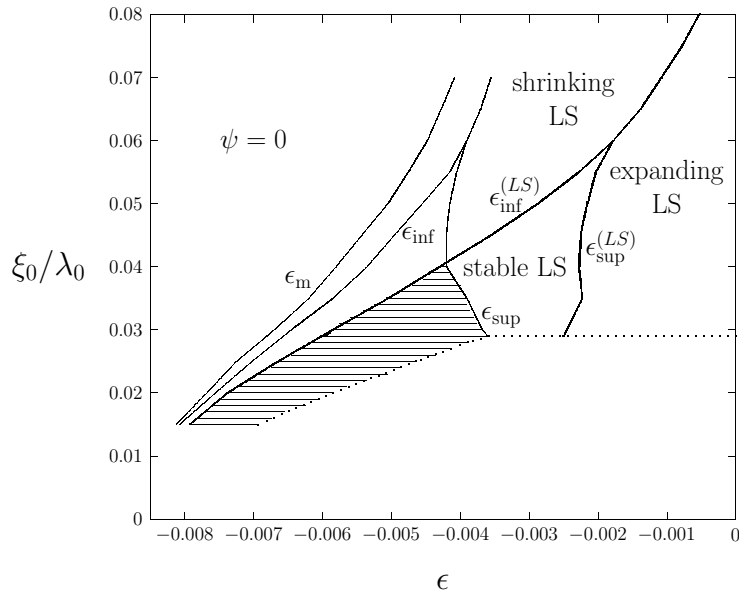


FIG. 8: Stability diagram of localized structures (LS), superposed to that of Figure 6 for planar fronts ($g_2 = 0.2$). In the hatched region, fronts are pinned and localized structures do not expand nor shrink, and therefore have an infinite life-time.

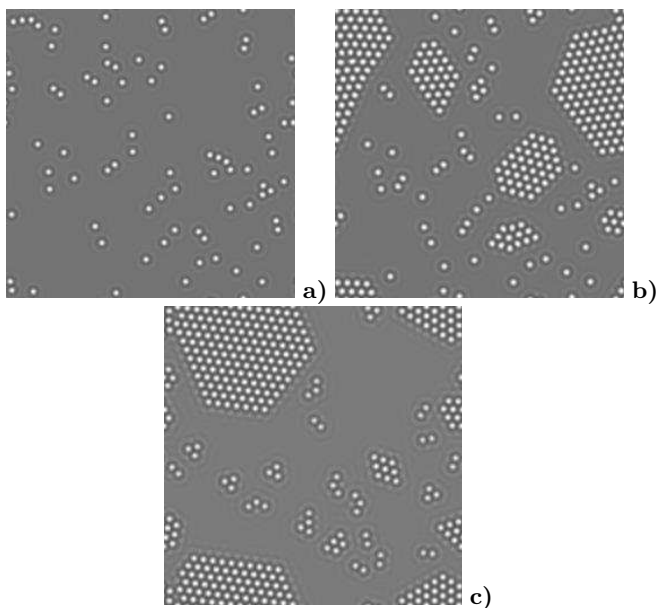


FIG. 9: Different kinds of frozen configurations of ψ (in gray scale) obtained at large times from random initial conditions ($g_2 = 0.2$). **a)** The coherence length is $\xi_0 = 0.031\lambda_0$ and $\epsilon = -0.0055$ is near $\epsilon_{\text{inf}}^{(LS)}$ in the hatched region of Figure 8 ($t = 20000$, $\alpha = 13$). **b)** Same ξ_0 , with $\epsilon = -0.0040$, closer to ϵ_{sup} in the hatched region of Figure 8 ($t = 240000$, $\alpha = 8.66$). The pinned hexagonal clusters are faceted, and stable localized structures are still observed. **c)** $\xi_0 = 0.04\lambda_0$ and $\epsilon_{\text{inf}} \leq \epsilon = -0.0045 \leq \text{Min}[\epsilon_{\text{inf}}^{(LS)}, \epsilon_{\text{sup}}]$: interfaces are pinned but localized structures are unstable (shrink). The smallest stable structures are clusters with two dots.

blies of localized structures of liquid-like character, with no visible hexagonal order. The example shown in Figure 9a at $\epsilon = 0.0055$ (for a system of size 256×256) is similar to the patterns presented in various studies on “spatial chaos” [8, 11, 12]. Given a random initial condition, at short times, most of the pattern quickly relax to the conductive state $\psi = 0$, with only a few remaining patches that further lead to immobile localized structures. One can control the final density of localized structures by means of the parameter α in the initial condition. The configurations become more dilute as α decreases.

If ϵ is increased and set closer to ϵ_{sup} in $[\epsilon_{\text{inf}}^{(LS)}, \epsilon_{\text{sup}}]$, random initial conditions gradually tends to form other kinds of frozen disordered states. These states are “mixed”, characterized by the presence of both localized structures and faceted extended hexagonal domains (Figure 9b). The interfaces in Fig. 9b are pinned, as expected. The enhancement of hexagonal order for quenches closer to ϵ_{sup} can be qualitatively understood from Section III B: the driving force F increases with ϵ faster than the pinning potential p , even in the pinning zone, see Fig.2. The time evolution of a typical configuration is the following: A few stable localized structures form at intermediate times. Small clusters, composed of 2,3,4 or more dots, are also present. Clusters with 2 dots do not grow (nor move). Some clusters with 3 or more dots are unstable: some of them, that are initially irregular, expand slowly by the creation of successive layers of dots (they may absorb in the process stable localized structures standing in their neighborhood). Growing clusters eventually reach steady states, corresponding to faceted polygons with an underlying hexagonal structure. These extended hexagonal domains (generalizations of

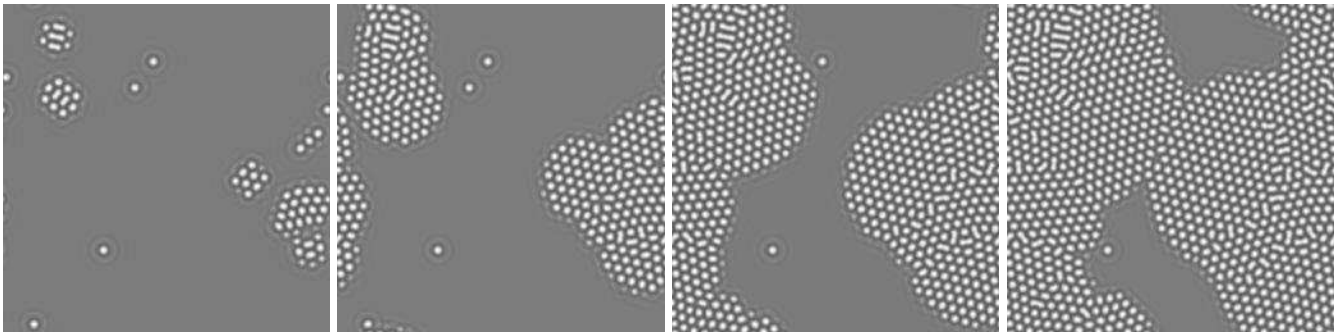


FIG. 10: Pattern evolution for $\epsilon_{\text{sup}} < \epsilon = -0.0026 < \epsilon_{\text{sup}}^{(LS)}$. (The other parameters are $\xi_0 = 0.031\lambda_0$ and $g_2 = 0.2$.) Four successive configurations of a same run are shown, respectively at times $t = 5000, 10000, 15000, 20000$. Localized structures are stable, but eventually absorbed by the growing domains.

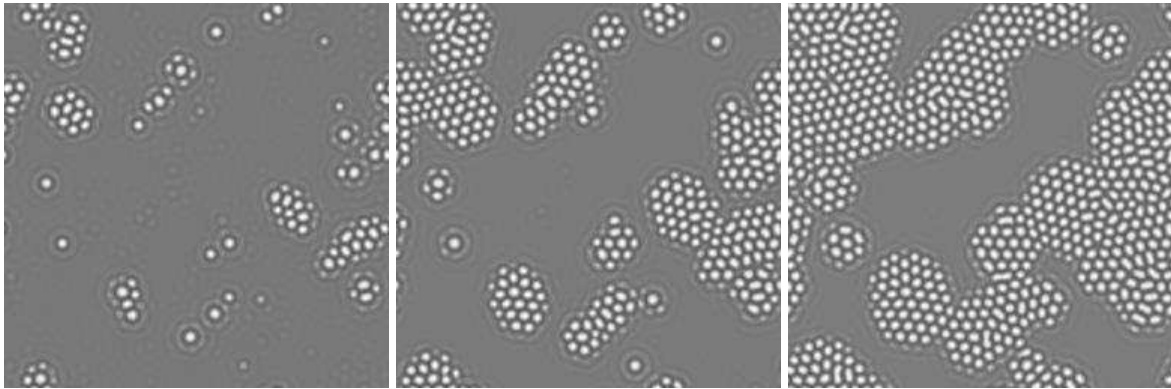


FIG. 11: Same parameters as in Figure 10, with $\epsilon = -0.0010 > \epsilon_{\text{sup}}^{(LS)}$. Three successive configurations at times $t = 2000, 3000, 4000$ are displayed. Transient localized structures are now unstable, and nucleate fast-growing hexagonal domains.

the 7-dots structures observed in ref.[12]) coexist with the remaining single localized structures. It takes a long time (typically 300,000 times units) for the whole system to reach a steady state. The normal to an interface can be directed along non-crystalline directions, due to, for instance, merging processes taking place between neighboring clusters. Domains can be fairly extended by the time they reach a faceted shape, that further prevent their growth.

The facets ensure stability, although some defects (penta-hepta dislocations) can be present in the bulk of a domain. A slight cusp inward is visible on an interface in the upper left corner of Fig.9b. This feature is reminiscent of a grooving effect with sharp angles, a phenomenon well known in polycrystals with a strong anisotropy in surface tension [28].

Further increase in ϵ beyond ϵ_{sup} leads, as expected, to homogeneous states of hexagons, with no conductive regions at large times. Figure 10 shows successive configurations obtained at intermediate times in the case $\epsilon_{\text{sup}} \leq \epsilon (= -0.0026) \leq \epsilon_{\text{sup}}^{(LS)}$. Small hexagonal clusters grow, in a way analogous to a stable phase in a metastable one. Although the single localized structures present are individually stable, they are absorbed during growth, as hexagon/uniform interfaces sweep them

in a finite time. Hence, localized structures can not be observed at arbitrary large times and are metastable in this range. The “absolute” stability region of localized structures is in practice restricted to the hatched zone of Fig.8, included in the pinning zone of interfaces.

When the control parameter exceeds $\epsilon_{\text{sup}}^{(LS)}$, transient short-lived localized structures may still emerge from random initial conditions. They further destabilize by forming structures of six-fold symmetry and then growing bubbles, as illustrated in the sequence of Figure 11. Localized structures nucleate hexagonal order in this case, as already observed in the Lengyel-Epstein model of Turing patterns [13] and experimentally in semiconductor-gas discharge systems [7].

An other possible case, illustrated by Figure 9c, corresponds to pinned interfaces and unstable (shrinking) localized structures. It happens in the roughly triangular region delimited by the curves ϵ_{inf} , ϵ_{sup} and $\epsilon_{\text{inf}}^{(LS)}$ in Fig.8. In Fig.9c, the smallest structures observed are clusters with two dots. Finally, for $\epsilon \leq \epsilon_{\text{inf}}$, any initial random condition converges toward the conductive state $\psi = 0$.

VI. CONCLUSIONS

We have studied the dynamics of interfaces in the bistability region of conductive and hexagonal states of the Swift-Hohenberg equation (1). We have examined the consequences of the various dynamical regimes of interfaces on the occurrence of spatial complexity and on the metastability of smaller structures like localized structures. Steady disordered states are possible in the nonlinear regime only, and for a choice of parameters such that planar interfaces remain pinned. In the expansion regime ($\epsilon > \epsilon_{\text{sup}}$) localized structure may be stable but are susceptible to be swept by any traveling interface in a finite time.

The size of the pinning interval $[\epsilon_{\text{inf}}, \epsilon_{\text{sup}}]$ is significant as soon as the bare coherence length ξ_0 is of the order of (or smaller than) a characteristic value $\xi_0^{(p)}$, approximately given by formula (21). An extended domain with pinned interfaces can be seen as a nonequilibrium analogue of a solid crystal. Domains can contain dislocations in the bulk, and even vacancies. Defects can induce grooving-like effects at the interface (non-planar interfaces with a cusp inward).

On general grounds, decreasing the coherence length ξ_0 (keeping the other parameters constant) increases nonlinear effects and enhances hexagonal order ($\psi(t = \infty) \neq 0$), as illustrated by the monotonic curves of $\epsilon_m(\xi_0)$ and $\epsilon_{\text{inf}}(\xi_0)$ in the diagram of Fig.6. The quantity ξ_0^{-1} can be seen as a measure of the pattern “strength”, a “weak” pattern yielding the phase $\psi = 0$. Though, one of the nontrivial features of Fig.6 is the *non-monotonic* behavior of ϵ_{sup} with ξ_0 . There exist a small interval of ϵ 's such that pinned states undergo a depinning transition (the system becoming completely filled with hexagons) if one slightly *increases* ξ_0 . In this case, a “weaker” pattern fills space better.

Heterogeneous frozen configurations can be of various kinds: they can include localized structures (“liquid”-like disorder), or both localized structures and extended faceted domains of the condensed phase (“mixed” disorder); or even, faceted domains with small clusters and no isolated localized structures. As the Swift-Hohenberg equation (1) is the minimal model allowing subcritical patterns and bistability, we expect the results presented here, specially the conclusions drawn from the diagrams of Figs.6 and 8, to be quite general and applicable to a variety of systems. Let us mention Turing chemical patterns, nonlinear optical systems and related devices [7, 12]. (Rayleigh-Bénard convection and block-copolymer melts are unfortunately less promising candidates as their ξ_0 is relatively large [3, 23].) Our results show in particular that crystal-like patterns can be con-

tained inside polygonal domains compatible with symmetries, and of arbitrary shape. Such patterns could be used as lithographic templates for technological applications (like micro-electronics) that require patterned surfaces over well-defined regions of space.

Acknowledgments

We thank M. Clerc for fruitful discussions. This work was supported by the Consejo Nacional de Ciencia y Tecnología (CONACYT, Mexico) Grant number 40867.

APPENDIX A: AMPLITUDE EQUATIONS WITH NON-ADIABATIC EFFECTS

The equations satisfied by the amplitudes A_n can be derived from Eq.(1) by standard multiple scale analysis [3]. The spatial variations of ψ , see Eq.(4), involve two kinds of length scales: a short scale associated with the periodicity of modulations, λ_0 , and a large one associated with the scale of variation of the amplitudes, of order L (the interface thickness). When $\epsilon \rightarrow 0$ and $g_2 \rightarrow 0$, $L \gg \lambda_0$, and it is possible to decompose spatial variations into “fast” variables, $\vec{r} = (x, y)$, and a “slow” variable $X = \epsilon^{1/2}x$ (as well a a slow temporal variable $T = \epsilon t$), such that $A_n = A_n(X, T)$. The equations for the A_n 's are derived from a solubility condition for ψ at the higher order following ψ_0 . The solubility condition for the amplitude A_n reads,

$$\int_x^{x+\lambda_0} \frac{dx'}{\lambda_0} \lim_{l_y \rightarrow \infty} \int_0^{l_y} \frac{dy'}{l_y} [L_n(\psi_0) + g_2 \psi_0^2 - \psi_0^3] e^{-i\vec{k}_n \cdot \vec{r}'} = 0, \quad (\text{A1})$$

where the linear operator $L_n = \epsilon - \epsilon \partial_T - \epsilon \xi_0^2 / (4k_0)^2 [2(\hat{k}_n \cdot \hat{x}) \partial_x \partial_X]^2$ follows from Eq.(1), ψ_0 being given by (4) and $\hat{k}_n = \vec{k}_n / |\vec{k}_n|$. In (A1), we have taken the limit $l_y \rightarrow \infty$ for commodity, since the interface profile is invariant along y . Close to onset, X and x can be considered as two independent variables and the only non-vanishing contributions of the integral (A1) come from the terms oscillating as $\exp(i\vec{k}_n \cdot \vec{r}')$ in the brackets. Coming back to physical variables, this leads to the well-known coupled amplitude equations (6)-(8)

According to relation (12), when ξ_0 is smaller than λ_0 (or when ϵ and g_2 are not small compared to unity), the “fast” and “slow” variables (x and X , respectively) can not be considered as independent in the solubility condition (A1) for A_n . ψ_0 being given by the decomposition (4), if one expands, for instance, the nonlinear term $g_2 \psi_0^2$ in Eq.(A1), some following integrals appear:

$$I = 2g_2 \int_x^{x+\lambda_0} \frac{dx'}{\lambda_0} \int_y^{y+\lambda_y} \frac{dy'}{\lambda_y} A_l(x') A_m(x') \exp(iK_x x') \exp(iK_y y') \quad (\text{A2})$$

with the notation $A_{-l} = \bar{A}_l$ and $-3 \leq m, l \leq 3$. In Eq.(A2), $\vec{K} \equiv K_x \hat{x} + K_y \hat{y} = \vec{k}_l + \vec{k}_m - \vec{k}_n$, with the notation $\vec{k}_{-l} = -\vec{k}_l$. This time, let us consider the non-resonant terms only, *i.e.* those with $\vec{K} \neq \vec{0}$. The A_n profiles of the planar interface depending on x' only, the contribution I is exactly zero unless $K_y = 0$. If $K_y = 0$ and $K_x \neq 0$, then I reduces to

$$I = 2g_2 \int_x^{x+\lambda_0} \frac{dx'}{\lambda_0} A_l(x') A_m(x') \exp(iK_x x'), \quad (\text{A3})$$

where K_x is actually a multiple (positive or negative) of k_0 . The usual amplitude formalism assumes that A_l varies slowly, so that $A_l(x') = \text{cst}$ in the interval $[x, x + \lambda_0]$. In that case, the non-resonant I given by Eq.(A3) always vanishes. However, as soon as L/λ_0 is large but finite, the complex exponential does not exactly integrate to zero if one sits in the interface region; I , although small, does not vanish.

Anticipating on Section III B (see Eq.20), one can show that a term like (A3) in the solubility condition (A1) gives an additional contribution of order

$$\frac{g_2 A_0^3}{D} \exp(-a|K_x|L) \sin(K_x x_0) \quad (\text{A4})$$

to the velocity v of the boundary given by Eq.(9). (See further Eq.(16)-(19).) In Eq.(A4), a is a constant of order unity, x_0 the position of the interface with respect to an arbitrary origin, and D given by (11). $|K_x|$ can take the values $k_0, 2k_0, 3k_0, \dots$. In (A4), $|K_x|L$ is finite but still assumed to be $\gg 1$: one can keep among the nonadia-

batic terms I those with the smallest $|K_x|$ ($|K_x| = k_0$), and neglect those involving higher wavenumbers.

One now derives the amplitude equations with their non-adiabatic corrections. One develops $g_2 \psi_0^2 - \psi_0^3$ (with ψ_0 given Eq.(4)), and, for each solubility condition (A1) ($n = 1, 2, 3$), one has to find out, with the notation introduced above, which are the products $A_l A_m$ (and $A_j A_l A_m$) such that $\vec{K} = \vec{k}_l + \vec{k}_m - \vec{k}_n$ (or $\vec{k}_j + \vec{k}_l + \vec{k}_m - \vec{k}_n$) has $K_y = 0$ and $K_x = \pm k_0$. Note that one must eliminate among the eligible products those that are resonant in any of the leading order amplitude equations (6)-(8) or their complex conjugates. These resonant terms, added to similar ones coming from the linear operator L_n in (A1), constitute one of the 6 standard amplitude equations: the sum of these terms cancels out at order $\epsilon^{3/2}$ (the order of the terms in the brackets of Eq.(A1)), and thus would contribute in non-adiabatic effects at the following order, not considered here. For example, in deriving the nonadiabatic contributions of the equation for A_2 , one finds an eligible term (A2) involving a product $A_1 A_2$, characterized by $|\vec{K}| = |\vec{k}_1| = k_0$. But this term is resonant in the equation for A_3 , and hence needs to be discarded. The products of amplitudes appearing in the leading nonadiabatic terms can not be already known products.

In order to calculate the integrals (A3), we next assume that the amplitudes vary slowly in the interval $[x, x + \lambda_0]$ and $A_n(x') \simeq A_n(x) + (x' - x) \partial_x A_n(x)$. After some tedious but straightforward algebra, equations (13)-(15) are obtained.

-
- [1] M.I. Rabinovich, A.B. Ezersky and P.D. Weidman, *The Dynamics of Patterns* (World Scientific, Singapore, 2000).
- [2] M. Cross and P. Hohenberg, *Rev. Mod. Phys.* **65**, 851 (1993).
- [3] P. Manneville, *Dissipative Structures and Weak Turbulence* (Academic, New York, 1990).
- [4] E. Bodenschatz, J.R. de Bruyn, G. Ahlers, and D.S. Cannell, *Phys. Rev. Lett.* **67**, 3078 (1991).
- [5] M. Assenheimer and V. Steinberg, *Phys. Rev. Lett.* **76**, 756 (1996).
- [6] F. Melo, P.B. Umbanhowar, H.L. Swinney, *Phys. Rev. Lett.* **75**, 3838 (1995).
- [7] Y.A. Astrov and Y.A. Logvin, *Phys. Rev. Lett.* **79**, 2983 (1997), and references therein.
- [8] O. Lejeune, M. Tlidi, and P. Couteron, *Phys. Rev. E* **66**, 010901 (2002).
- [9] P. Coulet, C. Elphick, and D. Repaux, *Phys. Rev. Lett.* **58**, 431 (1987).
- [10] S. Fauve and O. Thual, *Phys. Rev. Lett.* **64**, 282 (1990).
- [11] K.A. Gorshkov, L.N. Korzinov, M.I. Rabinovich, and L.S. Tsimring, *J. Stat. Phys.* **74**, 1033 (1994).
- [12] M. Tlidi, P. Mandel, and R. Lefever, *Phys. Rev. Lett.* **73**, 640 (1994).
- [13] O. Jensen, V.O. Pannbacker, E. Mosekilde, G. Dewel, and P. Borckmans, *Phys. Rev. E* **50**, 736 (1994).
- [14] V.J. Sánchez-Morcillo and K. Staliunas, *Phys. Rev. E* **60**, 6153 (1999).
- [15] Y.A. Astrov, *Phys. Rev. E* **67**, 035203 (2003).
- [16] Y. Pomeau, *Physica D* **23**, 3 (1986).
- [17] D. Bensimon, B.I. Shraiman, and V. Croquette, *Phys. Rev. A* **38**, 5461 (1988).
- [18] B.A. Malomed, A.A. Nepomnyashchy, and M.I. Tribelsky, *Phys. Rev. A* **42**, 7244 (1990).
- [19] C. Kubstrup, H. Herrero, and C. Pérez-García, *Phys. Rev. E* **54**, 1560 (1996).
- [20] I.S. Aranson, B.A. Malomed, L.M. Pismen, and L.S. Tsimring, *Phys. Rev. E* **62**, R5 (2000).
- [21] D. Boyer and J. Viñals, *Phys. Rev. E* **65**, 046119 (2002).
- [22] J. Swift and P.C. Hohenberg, *Phys. Rev. A* **15**, 319 (1977).
- [23] S.A. Brazovskii, *Sov. Phys. JETP* **41**, 85 (1975); G.H. Fredrickson, E. Helfand, *J. Chem. Phys.* **87**, 697 (1987).
- [24] D. Walgraef, *Spatio-Temporal Pattern Formation* (Springer Verlag, New York, 1996).
- [25] M. Cross, D. Meiron and Y. Tu, *Chaos* **4**, 607 (1994).
- [26] K.A. Jackson, *Am. Soc. Met.*, Cleveland, Ohio, p. 174 (1958).

- [27] C. Herring, *Structure and Properties of Solid Surfaces*, edited by R. Gomer and C.S. Smith (Univ. Chicago Press, 1952).
- [28] L.A. Wilen and J.G. Dash, *Science* **270**, 1184 (1995).